

Enhanced Molecular Orientation Induced by Molecular Anti-Alignment

E. Gershonabel and I. Sh. Averbukh

Department of Chemical Physics, The Weizmann Institute of Science, Rehovot 76100, ISRAEL

Robert J. Gordon

Department of Chemistry, University of Illinois at Chicago, Chicago, IL 60680-7061, USA

We explore the role of laser induced anti-alignment in enhancing molecular orientation. A field-free enhanced orientation via anti-alignment scheme is presented, which combines a linearly polarized femtosecond laser pulse with a half-cycle pulse. The laser pulse induces transient anti-alignment in the plane orthogonal to the field polarization, while the half-cycle pulse leads to the orientation. We identify two qualitatively different enhancement mechanisms depending on the pulse order, and optimize their effects using classical and quantum models both at zero and non-zero temperature.

PACS numbers: 33.80.-b, 02.30.Yy, 32.80.Lg

I. INTRODUCTION

The concept of molecular alignment refers to the angular localization of the symmetry axis of a molecule. The degree of alignment is measured by $\langle \cos^2 \theta \rangle$, where θ is the angle between the symmetry axis and a specified space-fixed axis, and $\langle \rangle$ denotes an average over the molecular ensemble. A molecule is said to be aligned if its symmetry axis lies along the space-fixed axis, whereas it is defined to be anti-aligned if its symmetry axis is perpendicular to the space-fixed axis. In recent years, various applications of molecular alignment have been proposed, including high harmonic generation [1], laser pulse compression [2], nanolithography [3], control of photodissociation and photoionization [4], and quantum information processing [5]. These applications have stimulated the need to align molecules optimally under field-free conditions. An important milestone in the development of alignment methods is the use of linearly polarized, ultra-short laser pulses to create a rotational wave packet by an impulsive Raman mechanism. If the temporal pulse width of the laser is shorter than the rotational period of the molecule (i.e., if its bandwidth is greater than the rotational level spacing), the molecule undergoes a series of Raman excitations that produce a coherent superposition of rotational states [6]. For short pulses, peak field-free alignment along the electric vector of the laser field is achieved after termination of the laser pulse, at a time that depends on the pulse strength. As the wave packet evolves, the molecule loses its alignment, and even becomes *anti-aligned* at some later time. The molecule also undergoes a series of field-free realignments [7] at integer multiples of the revival time, $\tau_{rev} = 1/(2Bc)$, where $B = \hbar/(4\pi c I_m)$ is the rotational constant, c is speed of light, and I_m is the moment of inertia. In addition, a number of fractional rotational revivals occur at rational fractions of τ_{rev} [8, 9].

Molecular orientation refers to the case of molecules with a directional symmetry axis (i.e., when a molecule has a permanent dipole). Orientation is measured by $\langle \cos \theta \rangle$, where θ is the angle between the molecular dipole

and the same spaced-fixed axis used to define alignment. Naturally, orienting a molecule requires breaking of the orienting field symmetry. Various symmetry-breaking methods have been proposed, including introduction of a weak DC electric (or magnetic) field in conjunction with a pulsed laser field [10], and coherent excitation with laser fields of frequencies ω and 2ω [11]. The most versatile method for orientating dipolar molecules utilizes asymmetric electromagnetic half-cycle pulses (HCPs) [12, 13]. Maximum field-free orientation is achieved some time after application of the HCP. A single short HCP has a limited effect, however. As was shown in ref. [13], its effect saturates with intensity. An HCP applied to a group of molecules that are initially oriented randomly in space contributes different angular velocities to individual molecules, so that molecules starting from obtuse angles ($\pi/2 \leq \theta \leq \pi$) move too slowly to catch up with molecules starting from acute angles ($0 \leq \theta \leq \pi/2$). As a result, the kicked molecules do not all point in the same final direction at any given time, and the orientation parameter has a maximum value of $\langle \cos \theta \rangle \approx 0.75$. This effect is similar to non-perfect focusing caused by spherical aberration in geometrical optics. It was shown theoretically [13, 14, 16] that the degree of field-free orientation and alignment can be enhanced by using trains of laser pulses, and enhanced alignment by a pair of pulses has been demonstrated experimentally [17, 18, 19, 20]. (For a recent review of field-free alignment, see Refs. [21, 22].) Creating a train of HCPs with sufficient strength to orient a molecule is experimentally difficult, however, requiring that alternative approaches be developed.

As we recently showed [23], anti-aligning molecules in a plane perpendicular to the HCP polarization can enhance the orienting effect of the HCP. In the current paper we investigate in detail the "orientation via anti-alignment" approach that combines an asymmetric half-cycle pulse with a symmetric femtosecond laser pulse. The latter induces *anti-alignment*, whereas the HCP orients the molecules. Depending on the pulse order, we identify two different mechanisms for enhanced field-free orientation,

and describe them qualitatively in section II. A rigorous formulation of the problem is given in III. A classical approach to the model at zero and finite temperatures is presented in section IV, and a full quantum treatment is developed in section V, where we also demonstrate further enhancement via a *three* pulse scheme. Finally, we summarize our findings in section VI.

II. "ORIENTING AN ANTI-ALIGNED STATE" AND "CORRECTING THE ROTATIONAL VELOCITY ABERRATION"

We identified two qualitatively different mechanisms for the orientation enhancement, which we term "orienting an anti-aligned state" and "correcting the rotational velocity aberration," depending on the temporal order of the pulses.

The "orienting an anti-aligned state" mechanism is illustrated in Fig. 1. The top drawing depicts a randomly oriented collection of molecules. A short symmetric laser pulse applied to the molecules pushes their symmetry axes toward the plane perpendicular to the desired orientation direction, preparing the molecules in an *anti-aligned state* angularly localized near $\theta = \pi/2$. A schematic illustration of the *anti-aligned state* is given in the middle drawing. When a delayed strong asymmetric HCP is applied to such an ensemble, all the molecules gain nearly the same rotational velocity. Because all the molecules depart from the anti-aligned state with very similar initial angles, they reach the orientation direction almost simultaneously at some later time, pointing in the same direction, as depicted in the bottom drawing. As is apparent from the bottom two drawings in Fig.

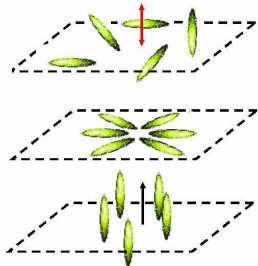


FIG. 1: "Orienting an anti-aligned state" mechanism. (Top) The symmetric pulse is applied to an ensemble of randomly oriented molecules. (Middle) After a time t_1 , when the molecules are anti-aligned, an asymmetric orienting pulse is applied. (Bottom) After an additional time t_2 , the molecules are oriented.

1, the more strongly the molecules are anti-aligned, the better they subsequently become oriented.

The "correcting the rotational velocity aberration" mechanism is illustrated in Fig. 2. First, we apply the asymmetric HCP. The molecules gain angular velocity in the direction illustrated in Fig. 2 by the filled arrows.

Then, shortly *after* the orienting HCP (or even simultaneously with it), we apply the symmetric laser pulse. Such a pulse decelerates the rotation of molecular dipoles having acute angles with respect to the orientation direction and accelerates those dipoles having obtuse angles. The directions of the angular velocity induced by the symmetric pulse is illustrated in Fig. 2 by the open arrows. This effect compensates for spherical aberration in the angular distribution of the rotational velocity distribution and improves the overall orientation at a later time.



FIG. 2: "Correcting the rotational velocity aberration" mechanism. Two schematic molecules are plotted. The filled arrows denote the first HCP orienting direction, and the open arrows denote the second symmetric pulse directions. The molecule at $\theta < \pi/2$ is decelerated by the symmetric pulse, whereas the molecule at $\theta > \pi/2$ is accelerated by the symmetric pulse.

In the following sections we demonstrate for both mechanisms that significantly enhanced orientation may be achieved by a proper choice of the delay between the pulses and of their relative intensities.

III. FORMULATION OF THE PROBLEM

The Hamiltonian of a 3D driven rigid rotor (linear molecule) interacting with a linearly polarized field is given by

$$H = \frac{\hat{J}^2}{2I_m} + V(\theta, t), \quad (1)$$

where \hat{J} is the angular momentum operator and θ is the angle between the molecular axis and the polarization vector of the field. For a symmetric laser pulse interacting with the induced polarization, the interaction term, averaged over the fast optical oscillations, is given by

$$V(\theta, t) = -\frac{1}{4}\varepsilon^2(t)[(\alpha_{\parallel} - \alpha_{\perp})\cos^2(\theta) + \alpha_{\perp}], \quad (2)$$

where $\varepsilon(t)$ is the envelope of the laser field, and α_{\parallel} and α_{\perp} are the parallel and perpendicular components of the polarizability tensor, respectively. For a symmetric laser pulse the contribution from the permanent dipole averages to zero.

For an asymmetric HCP, the interaction with the dipole moment is given by

$$V(\theta, t) = -\mu\varepsilon(t)\cos(\theta), \quad (3)$$

where μ is the permanent dipole moment and $\varepsilon(t)$ is the amplitude of the HCP. In the present paper we assume that the duration of the laser pulse is much shorter than the contributing periods of the rotational wave packet, so that the excitation dynamics may be calculated in the impulsive limit. The impulse imparted to the rotator is characterized by a dimensionless kick strength (or action), P . For an asymmetric pulse, P is given by

$$P_a = (\mu/\hbar) \int_{-\infty}^{\infty} \varepsilon(t) dt, \quad (4)$$

where the integration is performed over the unidirectional part of the HCP, and

$$P_s = (1/4\hbar)(\alpha_{\parallel} - \alpha_{\perp}) \int_{-\infty}^{\infty} \varepsilon^2(t) dt \quad (5)$$

for a symmetric pulse. We start with the mechanism of "orienting an anti-aligned state" and consider a rotator excited first with a symmetric pulse of strength P_s at $t = 0$ and then with an asymmetric pulse of strength P_a at $t = t_1$. Henceforth the dimensionless time is measured in the units of $I_m/\hbar = \tau_{rev}/2\pi$.

IV. CLASSICAL TREATMENT

Considerable physical insight may be derived from the (semi)-classical treatment of the problem, which is valid for $P_s, P_a \gg 1$. This is a natural approach to the process of enhanced orientation involving highly excited rotational states. In this section we formulate the orientation problem classically. A more general (although less intuitive) quantum mechanical treatment of the same problem is provided in section V. Classically, if a rotationless molecule is initially aligned at angle θ_0 , it will be found at the same angle just after the first symmetric kick (see Eqs.(2),(5)) but with angular velocity $-P_s \sin(2\theta_0)$, so that at some later time it will have an angle

$$\theta(t) = \theta_0 - P_s t \sin(2\theta_0). \quad (6)$$

When the orienting pulse of strength P_a is applied at time $t = t_1$, the velocity increment is $-P_a \sin[\theta(t_1)]$, so that the angular velocity after the second pulse is $\omega(\theta_0) = -P_s \sin(2\theta_0) - P_a \sin[\theta_0 - P_s t_1 \sin(2\theta_0)]$. The angle θ at time t_2 after the second pulse is therefore

$$\begin{aligned} \theta(t_1 + t_2) &= \theta_0 - P_s t_1 \sin(2\theta_0) - t_2 \{P_s \sin(2\theta_0) \\ &+ P_a \sin[\theta_0 - P_s t_1 \sin(2\theta_0)]\}. \end{aligned} \quad (7)$$

A similar expression may be derived for the inverse order of pulses, utilized in the second mechanism of enhanced orientation. The alignment at time $t = t_1$ and orientation at time $t = t_1 + t_2$ is calculated by averaging $\cos^k \theta(t)$ over all values of θ_0 ,

$$\langle \cos^k \theta(t) \rangle = \frac{1}{2} \int_0^\pi \cos^k \theta(t) \sin \theta_0 d\theta_0, \quad (8)$$

where $k = 1$ and 2 for orientation and alignment, respectively.

Our analysis shows that strong transient anti-alignment may be achieved via two related methods. The first one is of a classical nature. It operates on a short time-scale ($t \ll \tau_{rev}$) and requires *negative* values of the kick strength P_s . Pulses with negative P_s produce anti-alignment by pushing molecules into the equatorial plane ($\theta = \pi/2$). Fig. 3a shows the expectation value of $\langle \cos^2 \theta \rangle$ calculated both classically and quantum mechanically (as will be explained in section V) for a pulse with $P_s = -10$. Both treatments predict a deep minimum ($\langle \cos^2 \theta \rangle_{min} = 0.077$) shortly after the pulse at $t_m \approx 0.8/|P_s|$. There are various ways of achieving a *negative* kick strength of the symmetric pulse. First, some alkali halides (such as *LiF*) have a negative polarizability anisotropy ($\alpha_{\parallel} - \alpha_{\perp}$) [24]. Second, the interaction of molecules with a circularly polarized light pulse propagating in the direction of the desired orientation is proportional to $P_s \sin^2 \theta = P_s - P_s \cos^2 \theta$. This result is formally equivalent to the interaction with a linearly polarized pulse (our model) having negative kick strength.

A third method of achieving anti-alignment uses laser pulses with *positive* P_s , which cause a substantial *alignment* on a short (classical) time scale *after* the kick (see Fig. 3b). However, if it were possible to invert the dynamics and travel backwards in time, one would observe a strong anti-alignment *before* the kick. Remarkably, the effect of quantum revivals [9] provides such an option. Indeed, the rotational wave function satisfies the following equation

$$\Psi(\theta, \tau_{rev} - t) = \Psi(\theta, -t), \quad (9)$$

and, for sufficiently strong pulses, quantum dynamics just before one full revival cycle is equivalent to classical dynamics analytically continued to *negative* times. As a result, considerable anti-alignment is observed in this time domain (see Fig. 3b).

Next we would like to optimize the orientation factor $|\langle \cos(\theta) \rangle(P_s, P_a, t_1, t_2)|$ using the classical model (Eqs. (7) and (8)) with an anti-aligning pre-pulse ($P_s < 0$). In this procedure, the model is formally extended to negative times to cover effects in the full revival time-domain, as explained above. At zero initial temperature, the optimal solution depends only on the ratio P_a/P_s and the products $P_s t_1$ and $P_a t_2$. A contour plot of the orientation factor as a function of $|P_s|t_1$ and $|P_s|t_2$ (for a fixed ratio $P_a/|P_s| = 3$) is given in Fig. 4, where two almost equivalent extremum points are observed.

Figure 5 displays the highest (optimized with respect to the delay time) post-pulse orientation parameter, $\langle \cos \theta \rangle$ (solid line), and the optimal delay between pulses, t_{1opt} (dashed line), as functions of $P_a/|P_s|$. There are two optimal solutions of almost the same efficiency. The first one provides maximal orientation in the direction of the HCP shortly after the second pulse (upper panel in Fig. 5). The second one (lower panel in Fig. 5) delivers enhanced orientation in the *opposite* direction in the full

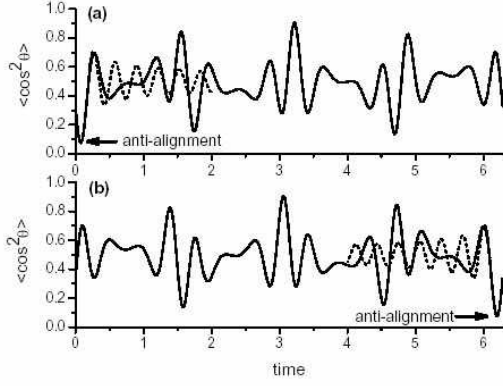


FIG. 3: Alignment parameter vs time after excitation by a laser pulse with (a) $P_s = -10$ and (b) $P_s = 10$. Solid curves are the quantum results. Dashed curves are calculated classically (a) for positive time and (b) for negative time (shifted by τ_{rev}). Strong anti-alignment is seen in both cases.

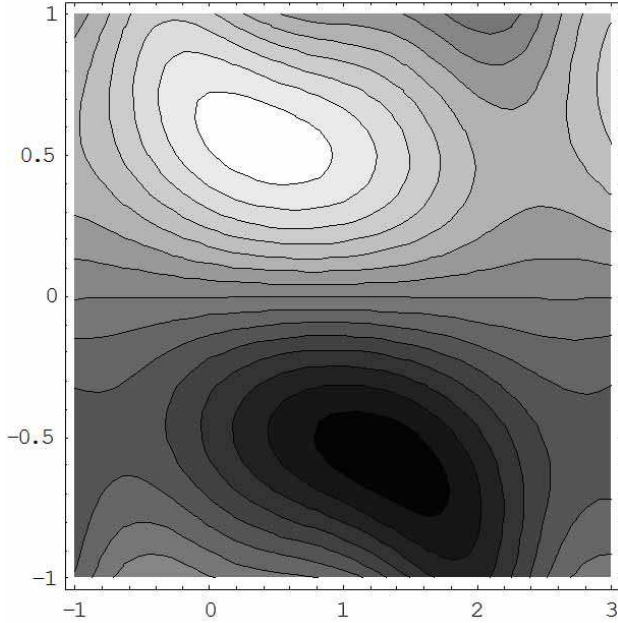


FIG. 4: Classical orientation factor as a function of $|P_s|t_1$ (horizontal axis) and $|P_s|t_2$ (vertical axis) for the first mechanism (the laser pulse precedes the HCP). $P_a/|P_s| = 3$. There are two almost equivalent extreme points.

revival domain after the second pulse. In both cases, an impressive value of $|\langle \cos \theta \rangle| \approx 0.95$ is achieved for rather modest pre-pulses ($|P_s| \sim 0.1P_a$) (as compared to the limit of $\langle \cos \theta \rangle_{max} \approx 0.75$ for a single HCP). In this regime, the optimal delay between pulses, i.e. optimal t_1 , asymptotically approaches the time of the best anti-alignment, $t_m \approx 0.8/|P_s|$.

It is easy to show that the same degree of orientation

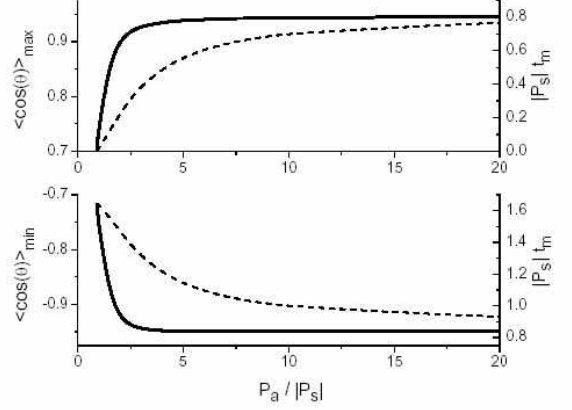


FIG. 5: Classically optimized orientation factor (solid curves) and delay between pulses (dashed curves). The laser pulse is fired before the half-cycle pulse.

may be achieved by combining an HCP with an aligning laser pulse ($P_s > 0$). The apparent symmetry relations,

$$\langle \cos \theta \rangle(P_s, P_a, -t_1, -t_2) = \langle \cos \theta \rangle(-P_s, -P_a, t_1, t_2) \quad (10)$$

and

$$\langle \cos \theta \rangle(P_s, P_a, t_1, t_2) = -\langle \cos \theta \rangle(P_s, -P_a, t_1, t_2), \quad (11)$$

reduce this problem to the already-studied case of the anti-aligning pulse.

We used the same approach to analyze the second mechanism of enhanced orientation mentioned in the Introduction. In the simplest, non-optimized version, the orienting and anti-aligning pulses are applied simultaneously ($t_1 = 0$). Direct numerical maximization of the expression in Eq. 8 shows that $\langle \cos \theta \rangle_{max} = 0.89$ when $P_a/|P_s| \approx 2.34$ and $|P_s|t_2 \approx 0.78$. When the hybrid pulse is composed of an orienting component and an *aligning* one ($P_s > 0$), the symmetry relations (10) and (11) predict the same orientation, but in the opposite direction ($\langle \cos \theta \rangle = -0.89$) just before one full revival cycle ($P_s t_2 \approx -0.78$). This effect was reported in a recent paper [25] as a result of direct numerical simulation of the quantum rotational dynamics of molecules excited by a single hybrid pulse. More efficient results may be obtained when the HCP precedes the anti-aligning laser pulse. In this case, our classical analysis reveals a single dominating optimal solution. A contour plot of the orientation parameter is given in Fig. 6. The optimal dominant solution is presented in Fig. 7. The maximum orientation $\langle \cos \theta \rangle_{max} \approx 0.96$ is reached at $P_a/|P_s| \approx 1.6$, and the optimal delay is $t_m \approx 0.36/|P_s|$.

As the next step, we calculate the orientation factor at a nonzero temperature. We shall derive the orientation factor for the "orientation of an anti-aligned state" mechanism only; the orientation factor for the second mechanism may be similarly derived.

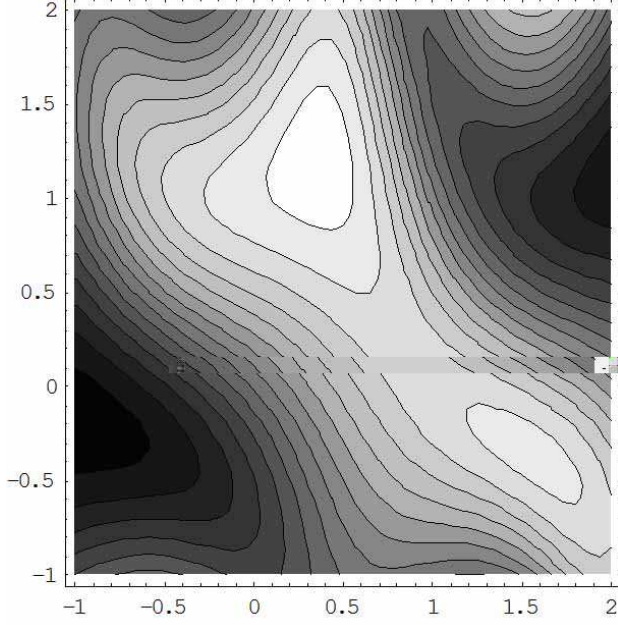


FIG. 6: Classical orientation factor as a function of $|P_s|t_1$ (horizontal axis) and $|P_s|t_2$ (vertical axis) for the second orientation mechanism (HCP precedes the laser pulse). $P_a/|P_s| = 1.6$. There is a single dominant maximum.

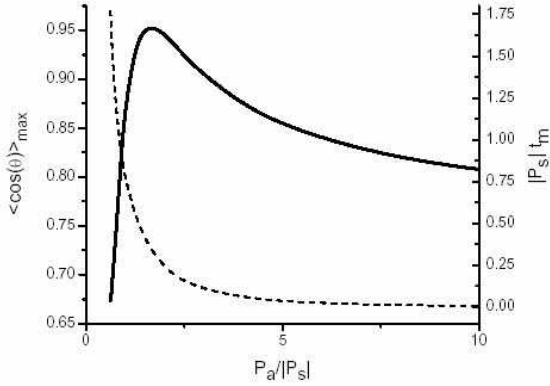


FIG. 7: Classically optimized orientation factor (solid curve) and delay between pulses (dashed curve). The laser pulse is fired after the half-cycle pulse.

The Lagrangian for the 3D free rotor is given by

$$L = \frac{1}{2}I_m(\dot{\theta}^2 + \dot{\phi}^2 \sin^2 \theta), \quad (12)$$

and the Euler-Lagrange equation for θ is

$$\frac{d}{dt} \frac{\partial L}{\partial \dot{\theta}} - \frac{\partial L}{\partial \theta} = 0. \quad (13)$$

The canonical momenta are

$$P_\phi = \frac{\partial L}{\partial \dot{\phi}} = I_m \dot{\phi} \sin^2 \theta, \quad (14)$$

(which is a constant of motion as ϕ is a cyclic coordinate), and

$$P_\theta(t) = \frac{\partial L}{\partial \dot{\theta}} = I_m \dot{\theta}. \quad (15)$$

From Eqs. (13), (14), and (15) the following equation of motion follows:

$$\ddot{\theta} = \frac{P_\phi^2 \cos \theta}{I_m^2 \sin^3 \theta}. \quad (16)$$

In what follows, it is convenient to measure the canonical momenta in the units of $p_{th} = I_m \omega_{th}$ with $\omega_{th} = \sqrt{k_B T / I_m}$, where T is the temperature and k_B is the Boltzmann constant. By setting $P'_\phi = P_\phi / p_{th}$, $P'_\theta = P_\theta / p_{th}$, and $t' = \omega_{th} t$, one writes Eq. (16) as

$$\ddot{\theta} = P_\phi'^2 \frac{\cos \theta}{\sin^3 \theta}. \quad (17)$$

The solution to this equation is

$$\begin{aligned} \cos \theta(t') &= \frac{1}{2} \left(1 - \frac{P'_\theta}{\omega}\right) \cos(\theta(0) - \omega t') \\ &+ \frac{1}{2} \left(1 + \frac{P'_\theta}{\omega}\right) \cos(\theta(0) + \omega t'), \end{aligned} \quad (18)$$

where

$$\omega = (P_\theta'^2 + \frac{P_\phi'^2}{\sin^2 \theta(0)})^{1/2}. \quad (19)$$

Here P'_θ is a constant initial canonical momentum (see Eq. (15)). As a result of a kick induced by a symmetric laser pulse applied at $t = 0$, P'_θ changes its value to

$$P'_\theta = P'_\theta(0) - P'_s \sin(2\theta(0)). \quad (20)$$

The initial thermal distribution function for the molecules has the following form in the chosen dimensionless variables:

$$f(\theta, \phi, P'_\theta, P'_\phi) = \frac{1}{8\pi^2} \exp\left[-\frac{1}{2}(P_\theta'^2 + \frac{P_\phi'^2}{\sin^2 \theta})\right]. \quad (21)$$

The thermally averaged alignment factor reads as

$$\begin{aligned} \langle \cos^2 \theta \rangle(t') &= \int_0^\pi d\theta(0) \int_0^{2\pi} d\phi(0) \int_{-\infty}^\infty dP'_\theta(0) \int_{-\infty}^\infty dP'_\phi(0) \\ &\times \cos^2 \theta(t') f(\theta(0), \phi(0), P'_\theta(0), P'_\phi(0)), \end{aligned} \quad (22)$$

where f is given by Eq. (21). The factor $\cos \theta(t')$ is provided by Eq. (18), in which $P'_\phi = P'_\phi(0)$, and P'_θ is given by Eq. (20). An HCP is applied with a delay t'_1 after the first symmetric laser pulse. Using the equations

$P'_\theta = \dot{\theta}$ and $d(\cos\theta)/dt = -\sin\theta\dot{\theta}$ we obtain P'_θ after the second pulse:

$$P'_\theta = -\frac{d(\cos\theta)/dt}{\sin\theta} - P'_a \sin\theta. \quad (23)$$

Here $\sin\theta$ and $\cos\theta$ are obtained from Eq. (18) at $t' = t'_1$. The new value of P'_θ and the angle $\theta(t'_1)$ are substituted again into Eq. (18) to propagate the rotation angle further. Thus, the time-dependent orientation factor is given by

$$\begin{aligned} \langle \cos\theta \rangle(t'_1 + t'_2) &= \int_0^\pi d\theta(0) \int_0^{2\pi} d\phi(0) \\ &\times \int_{-\infty}^\infty dP'_\theta(0) \int_{-\infty}^\infty dP'_\phi(0) \\ &\times \cos\theta(t' = t'_1 + t'_2) \\ &\times f(\theta(0), \phi(0), P'_\theta(0), P'_\phi(0)). \end{aligned} \quad (24)$$

From here on, we return to the previous dimensionless units used in this paper. In particular, the dimensionless kick strengths are replaced by

$$P'_{a,s} = P_{a,s} \frac{\hbar}{\sqrt{k_B T I_m}}. \quad (25)$$

Figure 8 displays a comparison between quantum (see the next section) and classical calculations for KCl molecule kicked by two coinciding pulses ($t_1 = 0$) at $T = 5K$. One may observe that the classical and quantum results agree well for strong pulses ($P \gg 1$) and short propagation time.

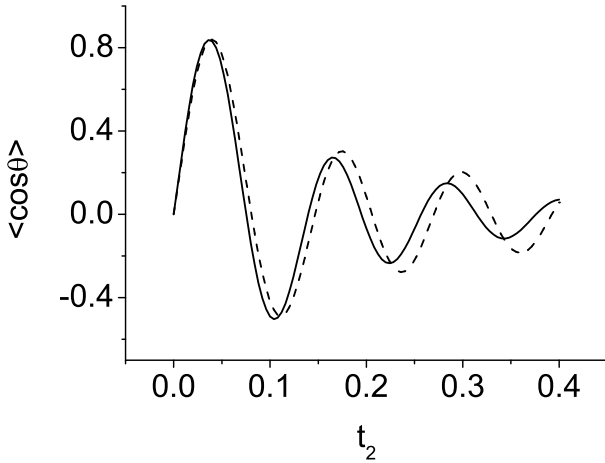


FIG. 8: Orientation parameter vs. t_2 ($t_1 = 0$) for $T = 5K$, $P_1 = -10$, and $P_2 = 50$. Solid and dashed lines are quantum and classical calculations, respectively.

V. QUANTUM TREATMENT

Consider a quantum rotator being initially in the ground state and kicked by a short symmetric laser pulse

at $t = 0$. In the impulsive approximation, its wave function acquires a phase factor as a result of the kick:

$$\Psi(\theta, t = +0) = \exp[iP_s \cos^2\theta] Y_0^0(\theta). \quad (26)$$

By expanding this expression as a sum of spherical harmonics, one finds the wave function at later time t :

$$\Psi(\theta, t) = \frac{1}{\sqrt{4\pi}} \sum_{J=0} c_J \exp[-iJ(2J+1)t] Y_{2J}^0(\theta). \quad (27)$$

The coefficients c_J are given by [14]

$$\begin{aligned} c_J &= \sqrt{\pi(4J+1)} (iP_s)^J \frac{\Gamma(J+1/2)}{\Gamma(2J+3/2)} \\ &\times {}_1F_1[J+1/2, 2J+3/2, iP_s], \end{aligned} \quad (28)$$

where ${}_1F_1$ is the confluent hypergeometric function. At $t = t_1$ the rotator is kicked by the orienting pulse, acquiring an additional phase factor

$$\Psi(\theta, t_1 + 0) = \exp[iP_a \cos\theta] \Psi(\theta, t_1 - 0). \quad (29)$$

We use the well-known expression

$$\exp(iP_a \cos\theta) = \sum_{J=0}^{\infty} i^J \sqrt{4\pi(2J+1)} j_J(P_a) Y_J^0(\theta), \quad (30)$$

where $j_J(P_a)$ is a spherical Bessel function, and again expand the wave function in a series of spherical harmonics

$$\Psi(\theta, t_1 + 0) = \sum_{l=0}^{\infty} d_l Y_l^0(\theta), \quad (31)$$

where

$$\begin{aligned} d_l &= \frac{1}{\sqrt{4\pi}} \sum_{l'=0}^{\infty} \sum_{j=0}^{\infty} i^j \sqrt{4\pi(2j+1)} j_j(P_a) c_{l'} \exp[-il'(2l'+1)t_1] \\ &\times \sqrt{(2j+1)(4l'+1)(2l+1)} \frac{C(j, 2l', l|0, 0, 0)^2}{2l+1}. \end{aligned} \quad (32)$$

Here $C(j, 2l', l|0, 0, 0)$ is a Clebsch-Gordan coefficient. This new wave function is allowed to propagate freely until $t = t_1 + t_2$, at which point the orientation and alignment parameters are calculated by

$$\langle \cos^k \theta \rangle = \langle \Psi(\theta, t) | \cos^k \theta | \Psi(\theta, t) \rangle, \quad k = 1, 2. \quad (33)$$

We performed a fully quantum-mechanical analysis of the "orientation via anti-alignment" and "correcting the rotational velocity aberration" mechanisms, using the above-described methodology. Figure 9 demonstrates the optimized values of the anti-aligning pulse strength, $|P_s|$, the optimum delay between pulses, t_m , and the maximal orientation parameter, $\langle \cos\theta \rangle_{max}$, as function of P_a . Very good agreement between quantum and classical results is observed even for moderate anti-aligning and orienting pulses ($P_s, P_a \sim 3$). Remarkably,

a significantly enhanced orientation may be achieved with field strengths available currently in the laboratory. Considering a KCl molecule in the ground state (having a revival time $t_{rev} \approx 128ps$, a dipole moment $\mu \approx 10.3D$, and a polarization anisotropy $(\alpha_{\parallel} - \alpha_{\perp}) \approx 3.1\text{\AA}^3$, data taken from [24]), one expects $P_a \sim 10$ for an HCP with the amplitude of $85kV/cm$ and a duration of about $2ps$ ($1/e$ half width). According to Fig. 9, the orientation factor $\langle \cos \theta \rangle \approx 0.95$ may be observed if the HCP is followed by a delayed anti-aligning pulse of $2ps$ duration and $5 \times 10^{11}W/cm^2$ peak intensity. Negative times in Fig. 9 correspond, as was explained above, to the dynamics in the full revival domain.

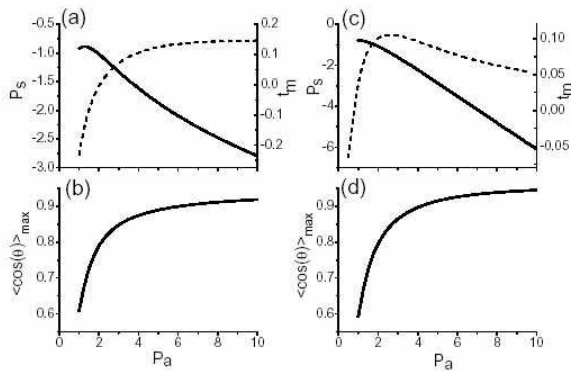


FIG. 9: Quantum mechanical optimized results at zero temperature. The left column (a,b) corresponds to the mechanism of "orienting an anti-aligned state" (laser pulse fired before the HCP). The right column corresponds to the mechanism of "correcting the rotational velocity aberration" (inverse order of pulses). Upper panels (a,c) display the optimal strength of the anti-aligning pulse (solid lines) and delay between pulses (dashed lines) as a function of the HCP strength. Lower panels (b,d) present the highest value of the post-pulse orientation factor vs the strength of the HCP.

We also analyzed quantum mechanically the orientation factor after two-pulse excitation for an ensemble having a non-zero temperature. The details of calculations can be found in the Appendix to this paper. The optimized solution for the orientation of an anti-aligned state is plotted in Fig. 10 as a function of P_a . A comparison between the classical and quantum thermal results was given in Fig. 8. One may observe in Fig. 10 that the temperature reduces the orientation effect. However, the latter is still considerably better compared to the single HCP excitation. The maximal orientation factor for KCl excited with a single HCP of strength $P_a = 10$ is 0.59 at $T = 5K$. The combined action of the HCP and laser pulse provides a much higher value of 0.69 at the same thermal conditions. To achieve even better orientation, one may try to add additional laser pulses to improve the

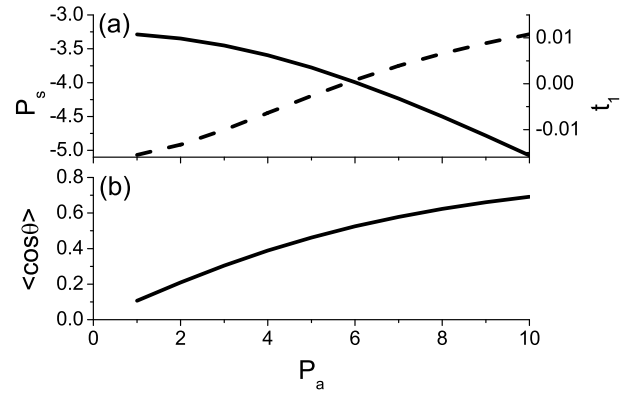


FIG. 10: Quantum mechanical optimized results for KCl at $T = 5K$. The graphs correspond to the mechanism of orienting an anti-aligned state (laser pulse fired before the HCP). a) Anti-aligning pulse strength and delay between pulses vs. HCP strength are given by solid and dashed lines, respectively. b) Orientation parameter vs. HCP strength.

anti-alignment in the system. The simplest scheme of this kind consists of two symmetric laser pulses separated by a delay t_1 , followed by an HCP after a second delay, t_2 . The optimal field-free orientation occurs at some time t_3 after the HCP. A full quantum optimization of this scheme at finite temperature presents a challenging numerical task, and goes beyond the framework of the present paper. The results of optimization at zero temperature are shown in Fig. 11. In particular, using the experimentally feasible HCP discussed above (i.e. $P_a = 10$ at $85kV/cm$) we obtain the optimized orientation factor $\langle \cos(\theta) \rangle = 0.97$ for $P_{s1} = -1.42$ and $P_{s2} = -3.95$. This means a 25% reduction in the width of the angular distribution compared to the two-pulse orientation scheme.

VI. CONCLUSIONS

We presented an experimentally feasible method for enhanced orientation of linear dipolar molecules using a half-cycle pulse combined with a delayed laser pulse inducing molecular anti-alignment. Two qualitatively different enhancement mechanisms were identified depending on the pulse order, and their effects were optimized with the help of quasi-classical as well as fully quantum models. The transparent physics behind the interplay between anti-alignment, orientation, and quantum rotational revivals provides a solid basis for the future design of more sophisticated and efficient solutions. In particular, we demonstrated that enforced anti-alignment by a pair of symmetric laser pulses prior to applying an HCP improves the orientation even more. These results may be generalized to trains of multiple laser pulses, similar to forced multi-pulse alignment techniques [13, 14, 15, 16, 17, 18, 19, 20]. In the same way, the "spherical aberrations" of a single HCP may be bet-

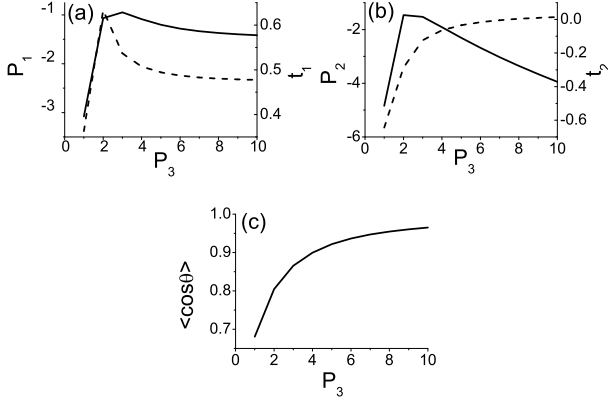


FIG. 11: Quantum mechanically optimized results for the three-pulse mechanism, where the first two pulses are symmetric, and the third pulse is an asymmetric HCP. a) First pulse strength P_1 and the delay between first and second pulses t_1 vs. HCP strength are given by solid and dashed lines, respectively. b) Second pulse strength P_2 and the delay between second and third pulses t_2 vs. HCP strength are given by solid and dashed lines, respectively. c) Orientation parameter vs. HCP strength.

ter corrected by multiple series of delayed laser pulses as well. Finally, a hybrid pair of delayed pulses may be followed by a series of well-timed symmetric laser pulses designed to preserve the achieved orientation over an extended time period [26, 27].

VII. ACKNOWLEDGMENTS

IA wishes to thank the Israel Science Foundation for support of this research, and RJG acknowledges the Motorola Corporation and the US Department of Energy for its support.

VIII. APPENDIX

We present here the finite-temperature results for the "orientation of an anti-aligned state" mechanism only. The orientation factor for the second orientation mechanism may be derived similarly.

At $T > 0$, the orientation factor should be thermally averaged over all initial states, so that

$$\langle \cos \theta \rangle = \sum_{l_0=0}^{\infty} P(l_0) \sum_{m_0=-l_0}^{l_0} A_{l_0}^{m_0}(t), \quad (34)$$

where

$$P(l_0) = \frac{1}{Q} \exp\left[-\frac{l_0(l_0+1)}{2\sigma_{th}^2}\right] \quad (35)$$

is the thermal distribution at temperature T , Q is the rotational partition function, and $\sigma_{th} = (k_B T / 2Bhc)^{1/2}$.

In Eq. (34),

$$A_{l_0}^{m_0}(t) = \langle \psi_{l_0}^{m_0}(t) | \cos(\theta) | \psi_{l_0}^{m_0}(t) \rangle \quad (36)$$

is the contribution to the orientation parameter from initial state $|l_0, m_0\rangle$.

The wave function $|\psi_{l_0}^{m_0}(t)\rangle$, is calculated as follows. After the first symmetric laser pulse, the wave function becomes

$$|\psi_{l_0}^{m_0}(0^+)\rangle = \exp[iP_s \cos^2(\theta)] |l_0, m_0\rangle. \quad (37)$$

Next, we expand $|\psi_{l_0}^{m_0}(0^+)\rangle$ in the spherical harmonic basis,

$$\psi_{l_0}^{m_0}(0^+) = \sum_{l=0}^{\infty} \alpha_l^{m_0} |l, m_0\rangle, \quad (38)$$

where the quantum number m_0 is preserved. The coefficient $\alpha_l^{m_0}$ may be derived by expanding $\exp[iP_s \cos^2(\theta)]$ in a sum of spherical harmonics using Eqs.(26),(27), and (28) and applying the rules of angular momentum algebra. However, we employ here another mathematically equivalent approach that is numerically advantageous for large values of P_s . For this, we expand $\exp[iP_s \cos^2(\theta)]$ in a series of Legendre polynomials, using the formula similar to Eq. (30), which gives (for negative P_s):

$$\begin{aligned} \exp[iP_s \cos^2(\theta)] &= \exp\left[-i\frac{|P_s|}{2}\right] \sum_{J=0}^{\infty} i^{3J} (2J+1) j_J\left(\frac{|P_s|}{2}\right) \\ &\times P_J(\cos(2\theta)). \end{aligned} \quad (39)$$

Next, we express $P_J(\cos(2\theta))$ as

$$P_J(\cos(2\theta)) = \sum_{L=0}^{\infty} d_{L,J} P_L(\cos \theta), \quad (40)$$

where the coefficients $d_{L,J}$ are generated by an efficient recurrent procedure described in Appendix A of Ref. [15]. Using the well-known relation between Legendre polynomials and spherical harmonics, one finds $\alpha_l^{m_0}$ to be

$$\begin{aligned} \alpha_l^{m_0} &= \exp\left[-i\frac{|P_s|}{2}\right] \sum_{J=0}^{\infty} \sum_{L=0}^{\infty} d_{L,J} i^{3J} (2J+1) \\ &\times j_J\left(\frac{|P_s|}{2}\right) \sqrt{\frac{2l_0+1}{2l+1}} \\ &\times C(L, l_0, l | 0, 0, 0) C(L, l_0, l | 0, m_0, m_0), \end{aligned} \quad (41)$$

where $C(L, l_0, l | 0, 0, 0)$, $C(L, l_0, l | 0, m_0, m_0)$ are Clebsch-Gordan coefficients. Free evolution after the first pulse gives

$$\psi_{l_0}^{m_0}(t_1^-) = \sum_{l=0}^{\infty} \alpha_l^{m_0} \exp\left[-\frac{i}{2}l(l+1)t_1\right] |l, m_0\rangle. \quad (42)$$

Next, we apply the second (asymmetric) pulse at time t_1 ,

$$\psi_{l_0}^{m_0}(t_1^+) = \exp[iP_a \cos(\theta)] \psi_{l_0}^{m_0}(t_1^-), \quad (43)$$

and again re-expand the new wave function,

$$\psi_{l_0}^{m_0}(t_1^+) = \sum_{\bar{l}=0}^{\infty} \tilde{\alpha}_{\bar{l}}^{m_0} |\bar{l}, m_0\rangle, \quad (44)$$

in order to find the spherical harmonic coefficients:

$$\begin{aligned} \tilde{\alpha}_{\bar{l}}^{m_0} &= \sum_{J=0}^{\infty} \sum_{l=0}^{\infty} i^J j_J(P_a) (2J+1) \alpha_l^{m_0} \exp[-il(l+1)\frac{t_1}{2}] \\ &\times \sqrt{\frac{2l+1}{2\bar{l}+1}} C(J, l, \bar{l}|0, 0, 0) C(J, l, \bar{l}|0, m_0, m_0). \end{aligned} \quad (45)$$

Finally, this new wave function propagates freely for a time interval t_2 , giving

$$\psi_{l_0}^{m_0}(t = t_1 + t_2) = \sum_{\bar{l}=0}^{\infty} \tilde{\alpha}_{\bar{l}}^{m_0} \exp[-\frac{i}{2}\bar{l}(\bar{l}+1)t_2] |\bar{l}, m_0\rangle. \quad (46)$$

This last expression is substituted into Eq. (36) in order to calculate the orientation factor given by Eq. (34).

-
- [1] R. Velotta, N. Hay, M. B. Mason, M. Castillejo, J. P. Marangos, Phys. Rev. Lett. **87**, 183901 (2001); J. Itatani, D. Zeidler, J. Levesque, M. Spanner, D. M. Villeneuve, and P.B. Corkum, Phys. Rev. Lett. **94**, 123902 (2005).
 - [2] R. A. Bartels, T. C. Weinacht, N. Wagner, M. Baertschy, C. H. Greene, M. M. Murnane, H. C. Kapteyn, Phys. Rev. Lett., **88**, 13903 (2002); V. Kalosha, M. Spanner, J. Herrmann, and M. Ivanov, Phys. Rev. Lett., **88**, 103901 (2002).
 - [3] R. J. Gordon, L. Zhu, W. A. Schroeder, and T. Seideman, J. Appl. Phys. **94**, 669 (2003).
 - [4] J.J. Larsen, I. Wendt-Larsen, H. Stapelfeldt, Phys. Rev. Lett. **83**, 1123 (1999); M. Tsubouchi, B. J. Whitaker, L. Wang, H. Kohguchi, and T. Suzuki, Phys. Rev. Lett. **86**, 4500 (2001); I. V. Litvinyuk, Kevin F. Lee, P. W. Dooley, D. M. Rayner, D. M. Villeneuve, and P. B. Corkum, Phys. Rev. Lett. **90**, 233003 (2003).
 - [5] E.A. Shapiro, M. Spanner, and M.Y. Ivanov, Phys. Rev. Lett., **91**, 237901 (2003); J. Mod. Optics, **52**, 897 (2005); K.F. Lee, D.M. Villeneuve, P.B. Corkum, E.A. Shapiro, Phys. Rev. Lett., **93**, 233601 (2004).
 - [6] J. P. Heritage, T. K. Gustafson, and C. H. Lin, Phys. Rev. Lett. **34**, 1299 (1975); J. Ortigoso, M. Rodriguez, M. Gupta, and B. Friedrich, J. Chem. Phys. **110**, 3870 (1999); T. Seideman, Phys. Rev. Lett. **83**, 4971 (1999).
 - [7] F. Rosca-Pruna and M. J. J. Vrakking, Phys. Rev. Lett. **87**, 153902 (2001).
 - [8] I.Sh. Averbukh and N.F. Perelman, Physics Letters A **139**, 449 (1989).
 - [9] For a recent review on quantum revivals, see R. W. Robinett, Phys. Rep. **392**, 1 (2004).
 - [10] B. Friedrich and D. Herschbach, J. Chem. Phys. **111**, 6157 (1999); J. Phys. Chem. A **103**, 10280 (1999); H. Sakai et al., Phys. Rev. Lett. **90**, 083001 (2003).
 - [11] E. Charron, A. Giusti-Suzor, and F. H. Mies, Phys. Rev. A **49**, R641 (1994); C. M. Dion, A. D. Bandrauk, O. Atabek, A. Keller, H. Umeda, and Y. Fujimura, Chem. Phys. Lett. **302**, 215 (1999); S. Gurin, L. P. Yatsenko, H. R. Jauslin, O. Faucher, and B. Lavorel, Phys. Rev. Lett. **88**, 233601 (2002); H. Ohmura and T. Nakanaga, J. Chem.Phys. **120**, 5176 (2004).
 - [12] C. M. Dion, A. Keller, and O. Atabek, Eur. Phys. J. D **14**, 249 (2001); M. Machholm and N. E. Henriksen, Phys. Rev. Lett. **87**, 193001 (2001).
 - [13] I. Sh. Averbukh and R. Arvieu, Phys. Rev. Lett. **87**, 163 601 (2001).
 - [14] M. Leibscher, I. S. Averbukh, and H. Rabitz, Phys. Rev. Lett. **90**, 213001 (2003); Phys. Rev. A **69**, 013402 (2004).
 - [15] M. Leibscher, I. S. Averbukh, P. Rozmej and R. Arvieu, Phys. Rev. A **69**, 032102 (2004).
 - [16] D. Sugny, A. Keller, O. Atabek, D. Daems, C. M. Dion, S. Gurin, and H. R. Jauslin, Phys. Rev. A **69**, 033402 (2004).
 - [17] K. F. Lee, I. V. Litvinyuk, P. W. Dooley, M. Spanner, D. M. Villeneuve, and P. B. Corkum, J. Phys. B: At., Mol. Opt. Phys. **37**, L43 (2004).
 - [18] C. Z. Bisgaard, M. D. Poulsen, E. Pronne, S. S. Viftrup, and H. Stapelfeldt, Phys. Rev. Lett. **92**, 173004 (2004).
 - [19] C. Z. Bisgaard, S. S. Viftrup, and H. Stapelfeldt, Phys. Rev. A **73**, 053410, (2006).
 - [20] D. Pinkham, and R.R. Jones, Phys. Rev. A **72**, 023418 (2005).
 - [21] H. Stapelfeldt, and T. Seideman, Rev. Mod. Phys. **75** (2003) 543.
 - [22] T. Seideman and E. Hamilton, Adv. At. Mol. Opt. Phys. **52**, 289 (2006).
 - [23] E. Gershnabel, I. S. Averbukh, and R. J. Gordon, Phys. Rev. A **73**, 061401(R) (2006).
 - [24] T. Pluta, Mol. Physics, **99**, 1535 (2001).
 - [25] D. Daems, S. Gurin, D. Sugny, and H. R. Jauslin, Phys. Rev. Lett. **94**, 153003 (2005).
 - [26] A. Matos-Abiague and J. Berakdar, Phys. Rev. A **68**, 063411 (2003).
 - [27] J. Ortigoso, Phys. Rev. Lett. **93**, 073001 (2004).